The 5th International Symposium - Supercritical CO_2 Power Cycles
March 28-31, 2016, San Antonio, Texas

THE EFFECT OF TEMPERATURE AND PRESSURE ON SUPERCRITICAL CO_2 COMPATIBILITY OF CONVENTIONAL STRUCTURAL ALLOYS

Bruce A. Pint
Group Leader
Oak Ridge National Laboratory
Oak Ridge, TN 37831-6156 USA
pintba@ornl.gov

Robert G. Brese
PhD student
University of Tennessee
Knoxville, TN 37996 USA
breserg@ornl.gov

James R. Keiser
Distinguished R&D Staff Member
Oak Ridge National Laboratory
Oak Ridge, TN 37831-6156 USA
keiserjr@ornl.gov

Bruce Pint is the Group Leader of the Corrosion Science & Technology Group in the Materials Science & Technology Division at ORNL. He received his Ph.D. from M.I.T. in Ceramic Science and Engineering in 1992 and has been at ORNL since 1994. Dr. Pint is the principal investigator for numerous R&D projects including corrosion issues in fossil energy, nuclear energy, fusion energy and combined heat and power systems. His research covers compatibility, lifetime predictions, environmental effects and coatings in all types of power generation. He is a Fellow of NACE International and ASM International.

Robert Brese is a Ph.D student in the Bredesen Center at the University of Tennessee studying Energy Science and Engineering. He earned his B.S. in Materials Science and Engineering from The Ohio State University in 2014. Robert joined the Corrosion Science & Technology group in 2015.

James Keiser is a Distinguished Research and Development Staff Member and has worked in ORNL's Corrosion Science & Technology Group since 1974 where he has studied the compatibility of materials with the environments of energy producing systems. Studies have addressed the performance of metallic and ceramic materials in environments containing gaseous, liquid and supercritical corrodents. Several of his current projects concern corrosion issues in biomass liquefaction and gasification. Dr. Keiser received his B.S. in Materials Science and Ph.D. in Metallurgical Engineering and is a Fellow of NACE International and ASM International.

ABSTRACT

There is considerable interest in both open and closed supercritical CO_2 (sCO_2) cycles but little information available on compatibility of conventional structural alloys in this environment. Initial screening experiments of 500 h have been conducted at 20 MPa at 400°-750°C to study the reaction rates and surface products formed. At the lower temperatures, 2-13%Cr steels were exposed, which tend to form duplex, Fe-rich surface oxide scales. At the higher temperatures, the focus was on higher-alloyed structural materials including high-strength Ni-base alloys, which generally are able to form a protective Cr- or Al-rich surface oxides. In addition, 500 h experiments were conducted at 750°C at 0.1-30 MPa, which included 25mm tensile bars of candidate alloys such as type 310 stainless steel, Ni-base alloy 740 and superalloy 247. A minimal effect of pressure was observed on the mass change and reaction products, similar to what was observed in

0.1 MPa dry air. Only minor changes in room temperature tensile properties were observed after these short exposures. Also, there was no indication of internal carburization and the Cr depletion in the precipitation strengthened Ni-base alloys (740 and 282) was minimal.

INTRODUCTION

Supercritical CO_2 (sCO_2) is being evaluated as a working fluid for a variety of nuclear, fossil, concentrated solar power (CSP), geothermal and waste heat recovery applications because of its unique properties and relatively low critical point (31°C/7.4 MPa) [e.g. Dostal 2006, Zhang 2006, Chen 2010, Gibbs 2010, Allam 2013, Iverson 2013, Wright 2013]. For fossil and CSP generation, the goal is to achieve system efficiencies of ≥50% with peak temperatures above 700°C and pressures of 20-30 MPa. Based on the experience of the U.S. Advanced Ultrasupercritical Steam Consortium [Viswanathan 2005, Viswanathan 2010], there are few material choices for long-term commercial power generation applications at >700°C and the leading candidates will be solid solution and precipitation-strengthened Ni-base alloys. However, unlike steam, there is virtually no compatibility data for structural alloys above 700°C in sCO_2. Figure 1 shows some of the prior data reported under supercritical conditions above 400°C [Oh 2006, Dunlevy, 2009, Gibbs, 2010, Rouillard 2011, Tan 2011, Moore 2012, Cao 2012, Firouzdor 2013, He 2014, Pint 2014a]. Compatibility is a concern in CO_2 environments because there is a long history of issues such as internal carburization of conventional austenitic steels discovered during the development of gas-cooled nuclear reactors with 0.1-4 MPa CO_2 environments [e.g. McCoy 1965, Evans 1976, Garrett 1982].

This study was launched in 2013 to begin screening compatibility of a wide range of structural alloys at higher temperatures and pressures for fossil energy applications above 700°C. The first step was the design of a Haynes 282 [Pike 2008] autoclave capable of achieving the target

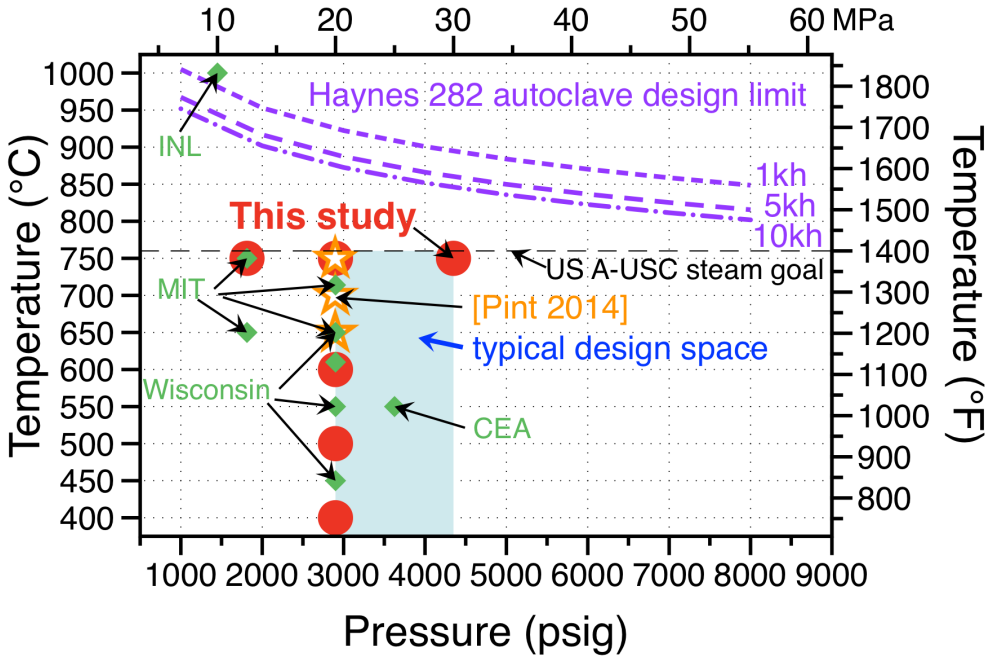

Figure 1. Previous and current sCO_2 studies as a function of CO_2 temperature and pressure. Diamonds show prior exposures at CEA [Rouillard 2011], INL [Oh 2006], MIT [Dunlevy 2009, Gibbs 2010] and Wisconsin [Tan 2011, Cao 2012, Firouzdor 2013, He 2014], stars show prior ORNL studies [Pint 2014a] and circles show current conditions. The design limits of the alloy 282 autoclave are shown for reference.

conditions, e.g. 760°C/30 MPa. The autoclave design limits are shown in Figure 1 along with the initial experimental conditions of 650°-750°C and 20 MPa reported previously [Pint 2014a]. The final phase of this work is reported here where (1) the effect of pressure was studied at 750°C from 0.1-30 MPa and (2) based on industry feedback, a range of Fe-base alloys was investigated at lower temperatures, 400°-600°C and 20 MPa to explore lower cost alloys for the lower temperature segments of the sCO_2 cycle. All of the data reported here are 500 h exposures and additional longer-term testing is needed to confirm these preliminary results.

EXPERIMENTAL PROCEDURE

The sCO_2 exposures were conducted in an autoclave fabricated from Haynes International alloy 282, a γ'-strengthened superalloy intended for high temperature structural applications [Pike 2008]. The vertically-oriented autoclave (~266 mm x 83 mm inner diameter) was operated inside a three-zone furnace with an alloy 282 sample rack that sat on the bottom of the autoclave. Supercritical fluid was supplied by a Supercritical model 24 constant flow dual piston pump at 1.0 mL/min and was fed into the autoclave through an alloy 625 supply tube that extended to within a few mm of the bottom of the autoclave. The autoclave pressure was controlled by a backpressure control valve which adjusted the orifice size as part of a feedback loop whose signal was based on the output of a pressure transducer located between the autoclave and the control valve. A rupture disc and a pressure relief valve were built into the same high-pressure line between the autoclave and the control valve to prevent an inadvertent over-pressurization of the system. Liquid CO_2 was provided from a cylinder containing CO_2 with a purity of at least 99.995% and <5 ppm moisture and <5 ppm total hydrocarbons specified. For these 500 h experiments, the specimens were slowly heated to temperature over several hours (~2°C/min) in sCO_2, held at temperature ±5°C and then cooled in sCO_2 to room temperature by lowering the furnace and using a cooling fan on

Table 1. Chemical composition of the alloys measured by inductively coupled plasma and combustion analyses in mass%.

Alloy	Fe	Ni	Cr	Al	Other
Ferritic chromia-forming steels					
Gr.22	95.5	0.2	2.3	<	0.9Mo,0.6Mn,0.1Si
Gr.91	89.7	0.1	8.3	<	1Mo,0.3Mn,0.1Si
VM12	83.3	0.4	11.5	<	1.6W,1.5Co,0.4Mo,0.4Mn,0.4Si,0.2V
410SS	86.9	0.1	11.8	<	0.5Mn,0.4Si
EBrite	72.6	0.1	25.8	<	1.0Mo,0.2Si,0.1V
Austenitic Fe-base chromia-forming steels					
201SS	70.8	4.1	16.2	<	6.7Mn,0.5Si,0.3Mo,0.9Cu,0.2Co
304H	70.4	8.4	18.4	<	1.6Mn,0.3Si,0.3Mo,00.4Cu,0.1Co
347HFG	66.0	11.8	18.6	0.01	1.5Mn,0.8Nb,0.4Si,0.2Mo,0.2Co
709	49.0	25.0	22.3	0.02	1.5Mo,1.0Mn,0.4Si,0.2Nb,0.2N
310HCbN	51.3	20.3	25.5	<	0.3Co,0.4Nb,1.2Mn,0.3Si,0.3N
Fe-base alumina-forming alloys					
APMT	69.2	0.2	21.1	5.0	0.2Hf,0.1Mn,2.8Mo,0.6Si,0.3Y,0.1Zr
Ni-base chromia-forming alloys					
625	4.0	60.6	21.7	0.09	9.4Mo,3.6Nb,0.2Ti,0.2Si,0.1Mn
230	1.5	60.5	22.6	0.3	12.3W,1.4Mo,0.5Mn,0.4Si
CCA617		0.6	55.9	21.6	1.3 11.3Co,8.6Mo,0.4Ti,0.1Si
282	0.2	58.0	19.3	1.5	10.3Co,8.3Mo,0.06Si,2.2Ti,0.1Mn
740	1.9	48.2	23.4	0.8	20.2Co,2.1Nb,2.0Ti,0.3Mn,0.5Si
Ni-base alumina-forming alloys					
214	3.5	75.9	15.6	4.3	0.2Mn,0.1Si,0.02Zr
247	0.07	59.5	8.5	5.7	9.8Co,9.9W,0.7Mo,3.1Ta,1.0Ti,1.4Hf

< indicates less than 0.01%

the autoclave. The comparison exposure at 1 bar was conducted in a horizontal alumina tube with end caps within a 3-zone furnace using the same CO_2 gas. In this case, the specimens were held in an alumina boat.

Table 1 lists the measured compositions of the alloys exposed in each condition. Alloy specimens were typically ~1.5 x 11 x 19 mm with a final 600 grit surface finish on all sides. All were evaluated in the as-received condition, including solution annealed condition for 740 and 282. The coupons were ultrasonically cleaned in acetone and methanol prior to exposure and suspended from alumina rods with alumina spacers between specimens. Mass change was measured on a Mettler Toledo model XP205 balance (±0.04 mg accuracy or ±0.01 mg/cm^2). After exposure, specimens were Cu-plated to protect the surface oxide and metallographically mounted and imaged with light microscopy. Subsequently, several specimens were investigated using a JEOL model 8200 electron probe microanalyzer (EPMA) using wavelength- and energy-dispersive x-ray spectrometers for chemical analysis. Tensile specimens were 25mm long (designated SS-3) with a gage of 0.8x5mm, a surface area of ~1.9 cm^2, and a 600 grit machined finish. The tensile tests were conducted at room temperature with a strain rate of 10^{-3} s^{-1}.

RESULTS

Figure 2 shows the mass change data measured at 400°-600°C in 20 MPa sCO_2 plotted versus the alloy Cr content. Similar mass change results for 650°-750°C and 20 MPa sCO_2 have been provided previously [Pint 2014a, Pint 2016a]. At 400°-600°C, more Fe-base alloys were exposed including 2.25%Cr Grade 22 steel. As expected, the measured mass change decreased with increasing Cr content, with the higher alloyed Fe- and Ni-base alloys showing very little mass gain after 500 h exposures at each temperature. Very little difference was seen between the mass change of the 9%Cr and 12%Cr ferritic-martensitic steel specimens (Grade 91 and VM12).

Figure 3 shows representative cross-sections of some of the Fe-base alloys exposed at 400°-750°C. A uniform duplex scale formed on the Grade 22 and 91 specimens at 400°-600°C with the oxide thicker on the 2.25%Cr steel as expected. Figure 4 summarizes the oxide thicknesses observed on the ferritic steel specimens where the scale was fully intact (i.e. no scale spallation).

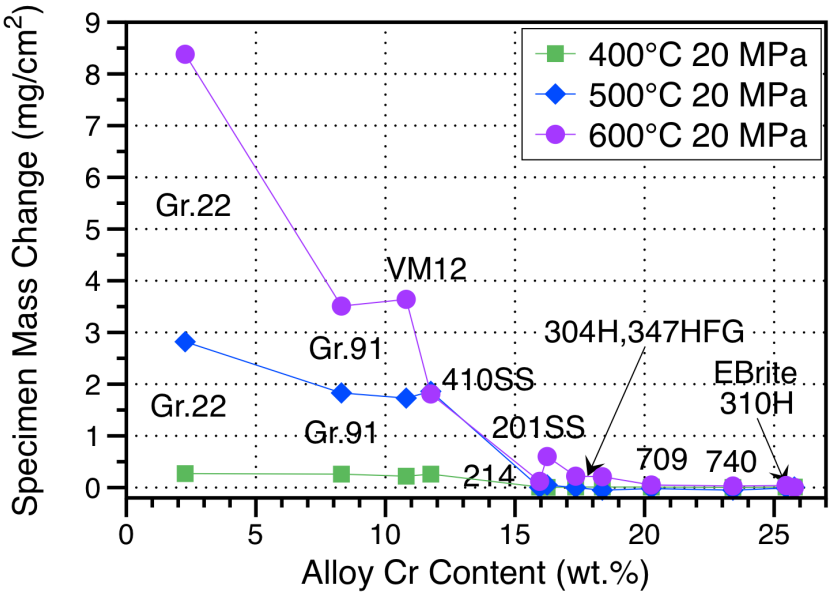

Figure 2. Specimen mass gain data as a function of alloy Cr content for 500 h exposures in 20 MPa sCO_2 at 400°-600°C.

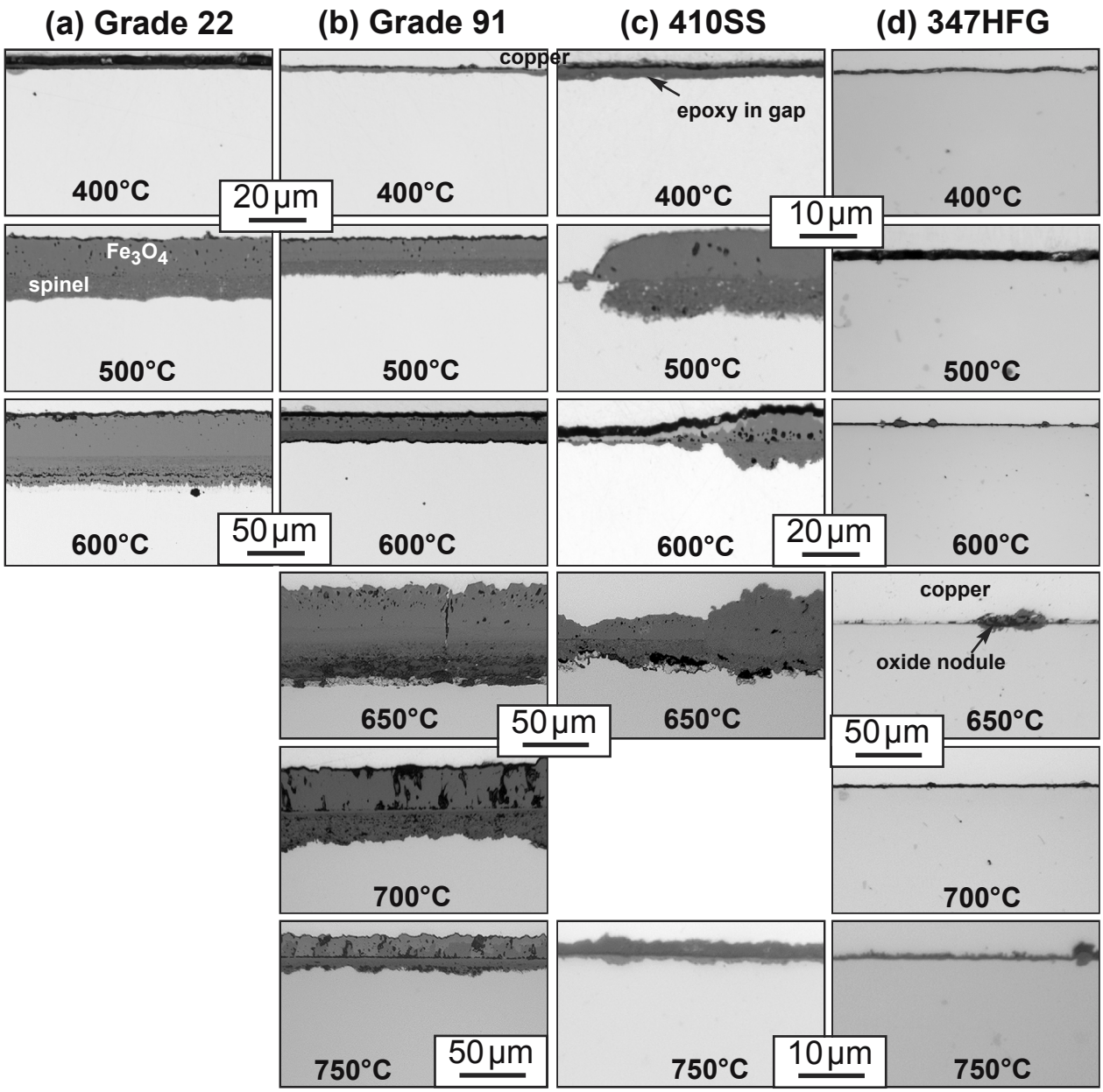

Figure 3. Light microscopy of polished cross-sections after 400°-750°C 20 MPa sCO_2 exposures for alloys (a) Grade 22, (b) Grade 91, (c) 410SS and (d) 347HFG.

Grade 22 and VM12 specimens were only exposed at 400°-600°C. As shown in Figure 3, a thicker scale formed on the 2.25%Cr Grade 22 specimens at 500° and 600°C. However, the 12%Cr VM12 specimen had a similar scale thickness as the 410SS and Grade 91 specimens at 600°C. A significant jump in oxide thickness on the Grade 91 and 410SS specimens was observed between 600° and 650°C, however, at higher temperatures the total oxide thickness was actual lower on both alloys. This may reflect faster diffusion of Cr at higher temperatures allowing a higher Cr content scale to form, especially on the higher Cr, 410SS specimen. It may also be a transient effect associated with a single exposure of 500 h. Additional testing is needed to verify this behavior.

Grade 91 was included over the entire temperature range as a comparison to several other sCO_2

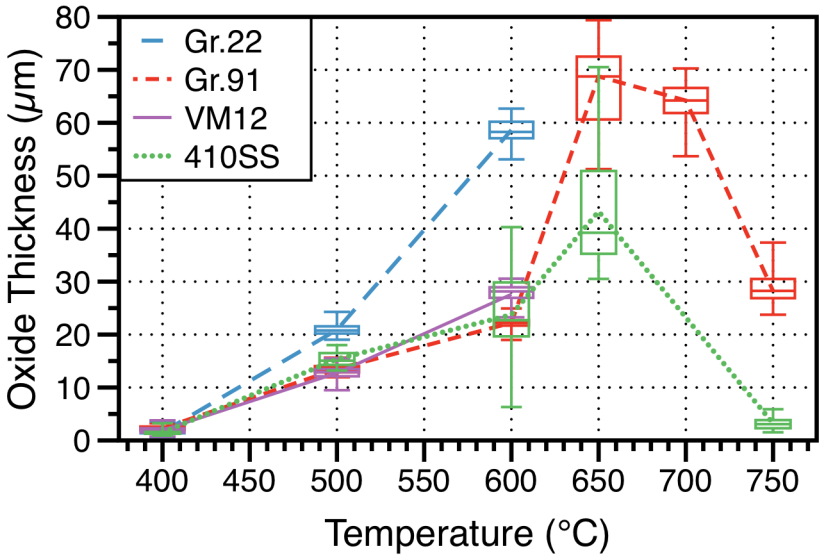

Figure 4: Box and whisker plot of oxide thickness for four Fe-Cr steels as a function of exposure temperature for the 500h exposures in 20 MPa sCO_2. The boxes show the 25%, median and 75% values measured and the whiskers the minimum and maximum values.

studies that have reported results on this alloy [Gibbs 2010, Rouillard 2011, Tan 2011]. In addition to the older work, more recent studies in 0.1MPa CO_2 have found internal oxidation of Fe-Cr steels [e.g. Gheno 2012]. The specimens exposed in this study have been evaluated by etching (Figure 5) and microhardness [Pint 2016b]. However, there was no indication of internal carburization. Figure 5b instead shows a carbide denuded zone at the metal-scale interface formed at 700°C,

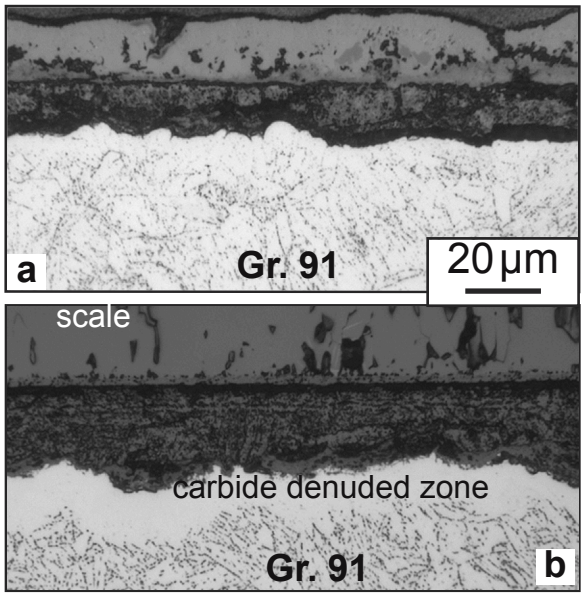

Figure 5. Light microscopy of polished and etched cross-section of Grade 91 (Fe-9Cr-1Mo) after 500 h at 700°C in (a) 0.1 MPa dry air and (b) 20 MPa. CO_2.

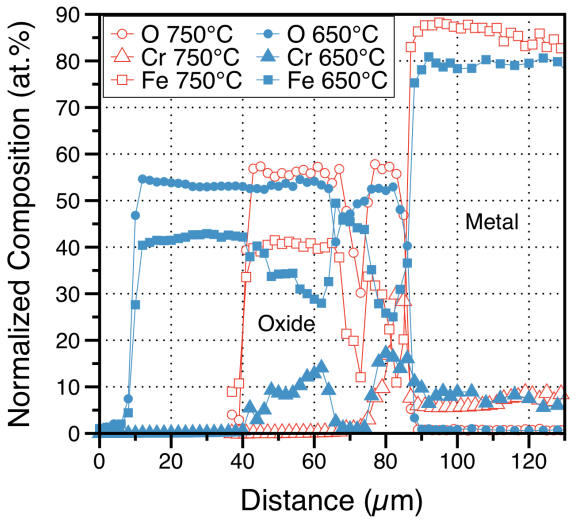

Figure 6. EPMA line profiles from G91 specimens exposed for 500 h at 650°C 20MPa and 750°C 30MPa.

with a larger zone formed at 750°C [Pint 2016b] consistent with Cr depletion to form the protective scale. Figure 5a shows a similar but narrower denuded zone formed in 0.1 MPa air after 500h at 700°C.

Figure 6 shows EPMA composition profiles through the scales formed on Gr.91 specimens exposed at 650° (20 MPa) and 750°C (30MPa). Typical of duplex oxides formed in air, humid air, steam and CO_2 [Wright 2010, Quadakkers 2011, Rouillard 2011, Pint 2014a, Pint 2014c], the outer oxide is FeO_x (typically a mixture of magnetite and haematite) and the inner oxide is a spinel-type oxide containing both Fe and Cr. Also typical of prior observations was an enrichment of Cr in the scale at the metal-oxide interface. As mentioned previously, the Cr enrichment was greater in the specimen exposed at 750°C, which may explain the thinner oxide formed at this temperature,

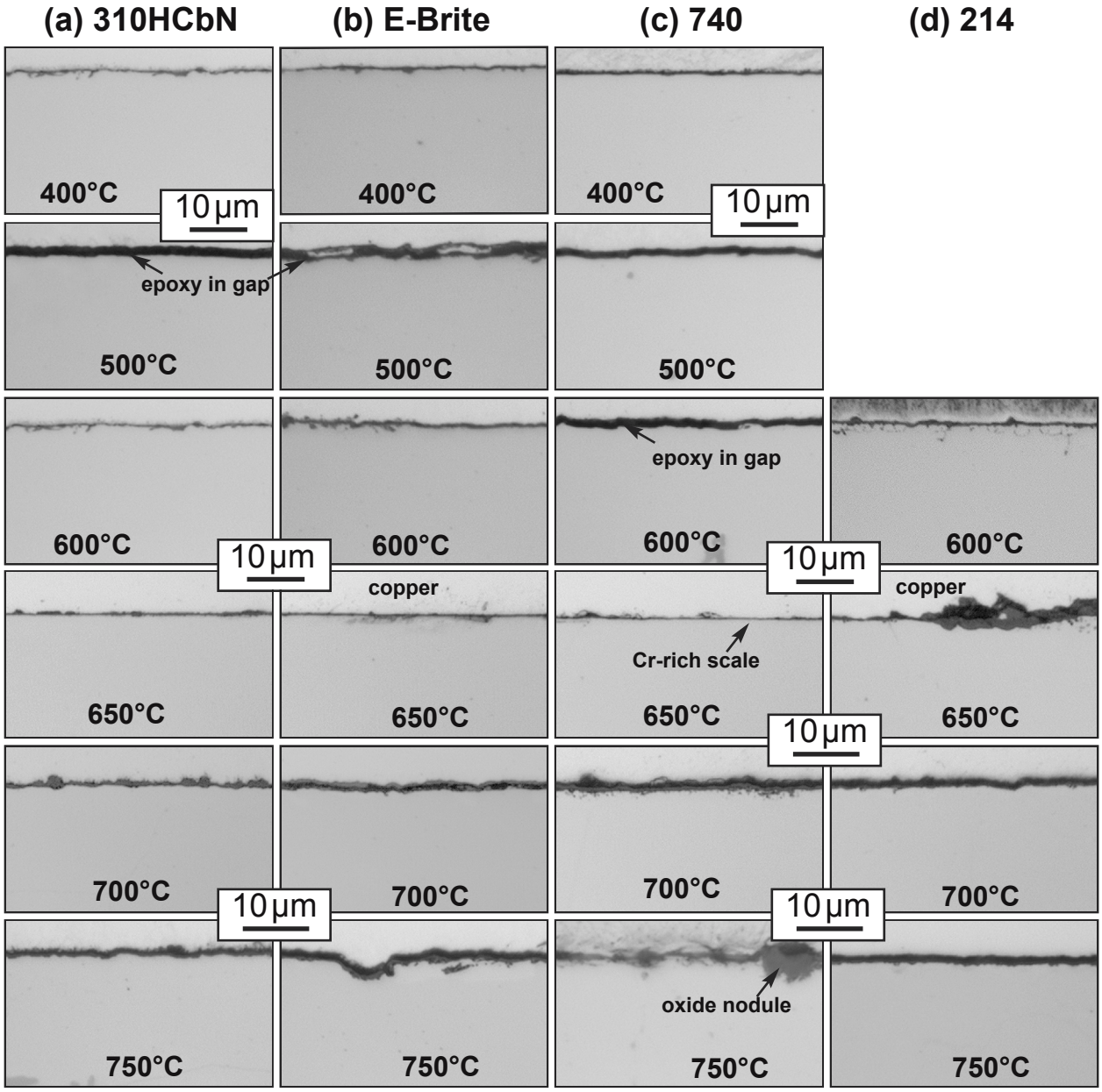

Figure 7. Light microscopy of polished cross-sections after 400°-750°C 20 MPa sCO_2 exposures for alloys (a) 310HCbN, (b) E-Brite (FeCr), (c) 740 and (d) 214

Figure 4. At higher temperature, the faster diffusion of Cr in the alloy may enable the formation of a more Cr-rich, protective scale compared to lower temperatures.

Figure 3d shows the scales formed on the 347HFG specimens at 400°-750°C. While some oxide nodules (with a similar duplex oxide structure as the Gr.91 specimens) were observed at 600°-750°C [Pint 2014a], a thin protective scale formed over most of the specimens. Figure 7 shows similar thin oxides formed on both the Fe- and Ni-based alloys over the same temperature range. Unlike the thick scales formed on the steel specimens, these thin oxides made characterization difficult by conventional microscopy. Very thin oxides were observed at 650°C except for the alumina-forming alloy 214, which surprisingly formed regions of thick oxide at this temperature. In these areas, the oxide was significantly thicker than the Cr-rich scale formed on the other alloys shown in Figure 7. This may be attributed to the relative slow diffusion of Al at this temperature inhibiting the formation of an Al-rich scale. At 700°C, thin oxides were observed in all cases. For the 750°C exposures, a slightly thicker Cr-rich oxide formed on most of the alloys with an occasional oxide nodule as is shown for alloy 740 in Figure 7.

The second phase of the study examined the effect of CO_2 pressure at 750°C. Figure 8 summarizes the mass change data for the 500 h exposures at 750°C in the 4 conditions studied. Except for the high mass gains for the Grade 91 specimens, the mass gains were generally low, suggesting thin protective Cr- or Al-rich oxides. The alloy 282 specimens exhibited higher mass gains than the other NiCr alloys. This difference may be attributed to the lower Cr content in this alloy compared to most of the other chromia-forming alloys, Table 1.

The characterization reported for this set of specimens focuses on the higher-alloyed structural alloys. The thick, duplex oxides formed on the Gr.91 specimens and the surprisingly thin oxides formed on 347HFG are reported elsewhere [Pint 2016b]. Figures 9 and 10 show examples of the thin oxides formed in this set of experiments. Several chromia-forming alloys are shown in Figure 9. (Because of the thin, relatively flat reaction products, adhesion of the Cu plating was an issue in some cases noted in Figures 9 and 10). While the mass gains were higher for alloy 282, Figure 8, the scale was not significantly thicker than the other alloys. Some of the increased mass gain for 282 can be attributed to the internal oxidation of Al and Ti, which form the γ′ strengthening

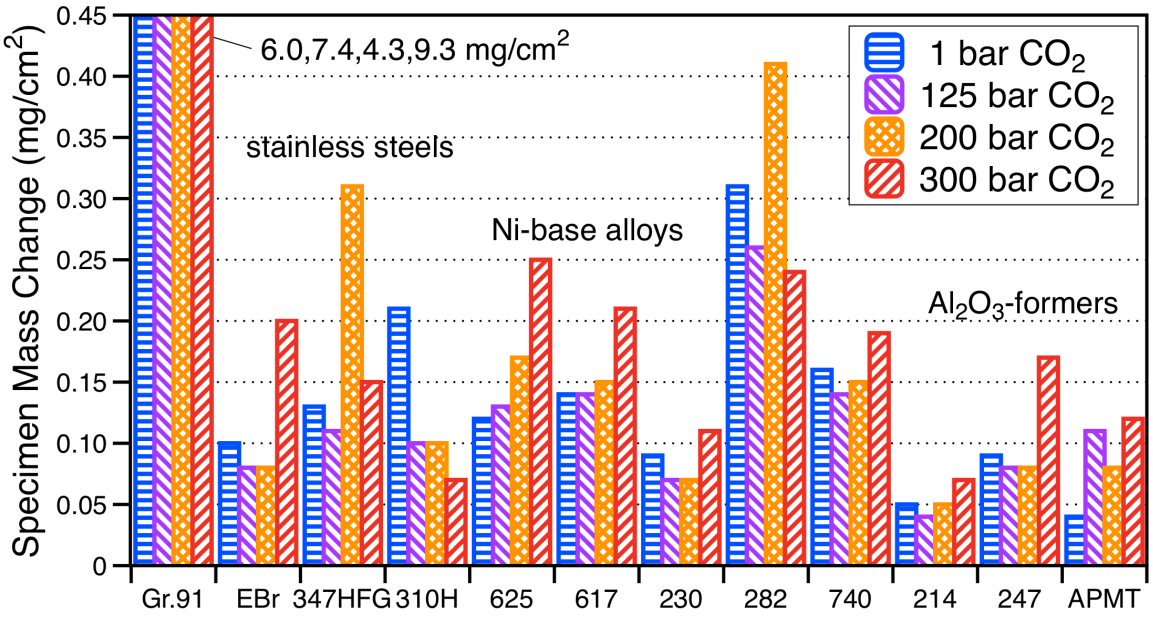

Figure 8. Specimen mass gain for 12 alloys exposed at 750°C for 500 h in four different CO_2 pressures from 0.1-30 MPa.

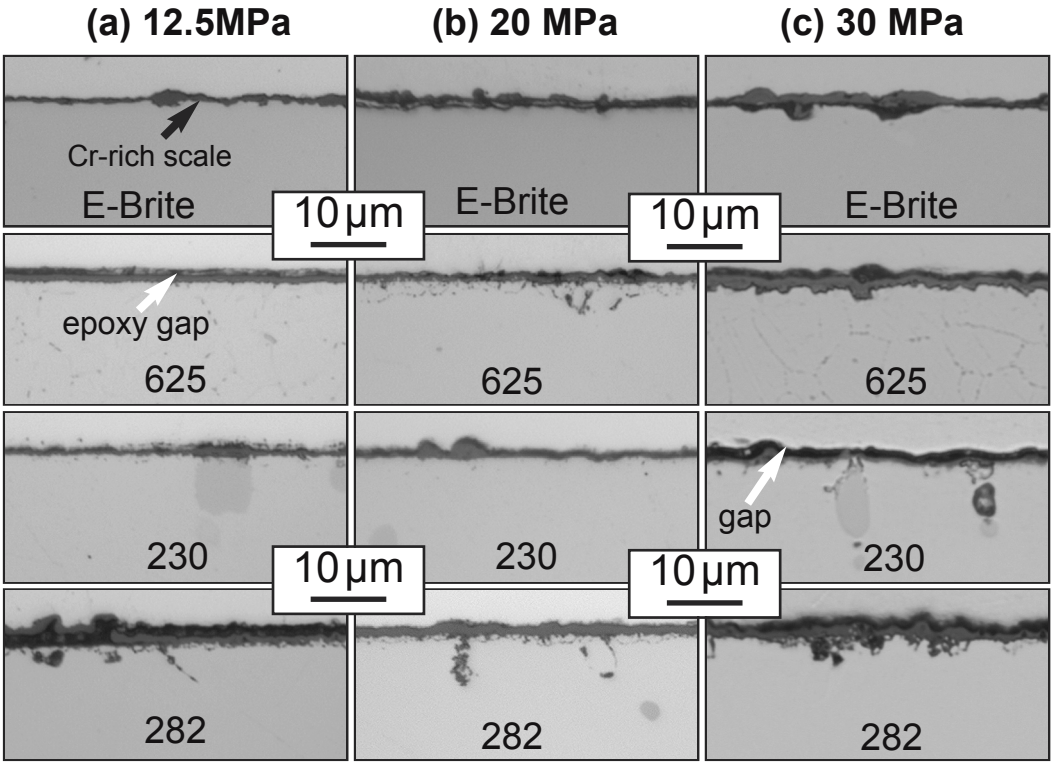

Figure 9. Light microscopy of polished cross-section of E-Brite, 625, 230 and 282 after 500 h at 750°C in CO_2 (a) 12.5 MPa, (b) 20 MPa and (c) 30 MPa.

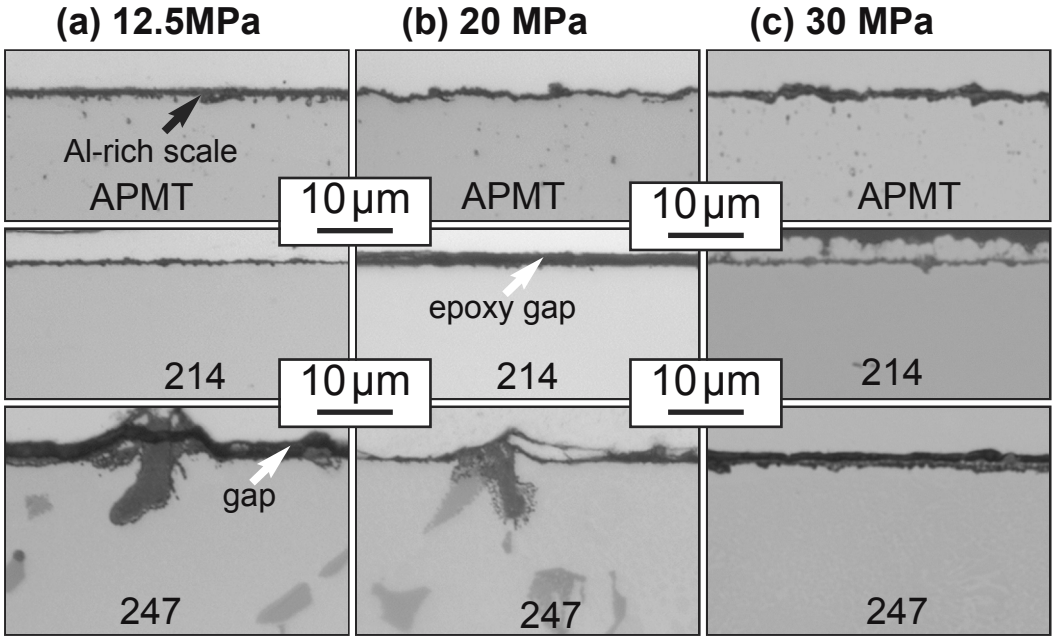

Figure 10. Light microscopy of polished cross-section of APMT, 214 and 247 after 500 h at 750°C in CO_2 (a) 12.5 MPa, (b) 20 MPa and (c) 30 MPa.

phase. A faster Cr_2O_3 growth rate also could be due to the higher Ti content in this alloy as Ti has been previously observed to increase the scale growth rate [Ennis 1985, Brady 2006, Pint 2014b]. Figure 11 compares the Cr depletion for alloy 282 and 740 specimens and uses 0.1 MPa dry air exposures as a baseline without carburization [Pint 2016b]. In one case at 20 MPa, the 282 specimen showed a much greater depth of Cr depletion than the alloy 740 specimen [Pint 2015a]. However, a much lower depletion depth was observed for 282 specimens exposed in air and 0.1 MPa CO_2. Additional characterization is needed to determine if the increased depletion can be attributed to the higher pressure or inhomogeneities associated with internal oxidation.

Figure 10 shows the thin Al-rich scales formed on Fe-based APMT and Ni-based 214 and 247 specimens. These thin oxides also are consistent with the low mass gains observed in Figure 8. The images for the alloy 247 specimens tend to focus on the Hf-rich carbides at the surface, Figure 10. The oxidation of these precipitates was characterized previously [Pint 2015a].

Finally, because of concerns of the sCO_2 environment affecting mechanical properties, small (25mm long) tensile specimens of 310HCbN, E-Brite, 740 and 247 also were exposed in these four environments at 750°C. Exposures of specimens as-received (baseline) and after 500h in air at 750°C are shown for reference, Figure 12. In general, the room temperature tensile properties of these alloys were relatively unaffected by these exposures. Alloy 740 likely "self-aged" under these conditions (i.e. γ′ coarsening [Shingledecker 2013]) resulting in a consistently higher ultimate tensile strength and lower ductility, independent of environment. The total elongation of the E-Brite specimens actually increased after most exposures.

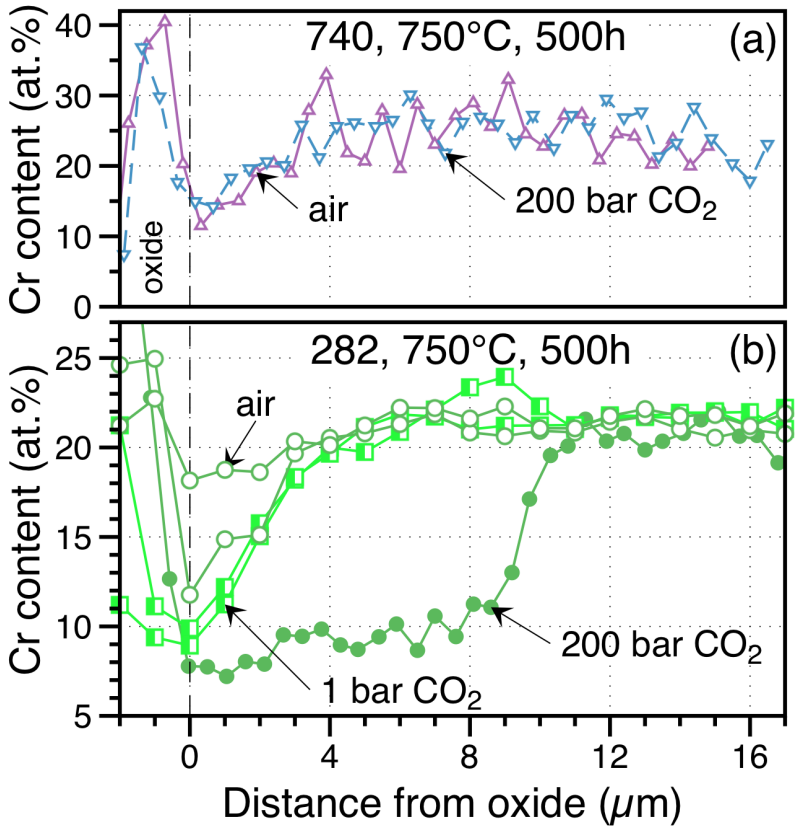

Figure 11. EPMA Cr line profiles from specimens exposed for 500 h at 750°C (a) alloy 740 and (b) alloy 282.

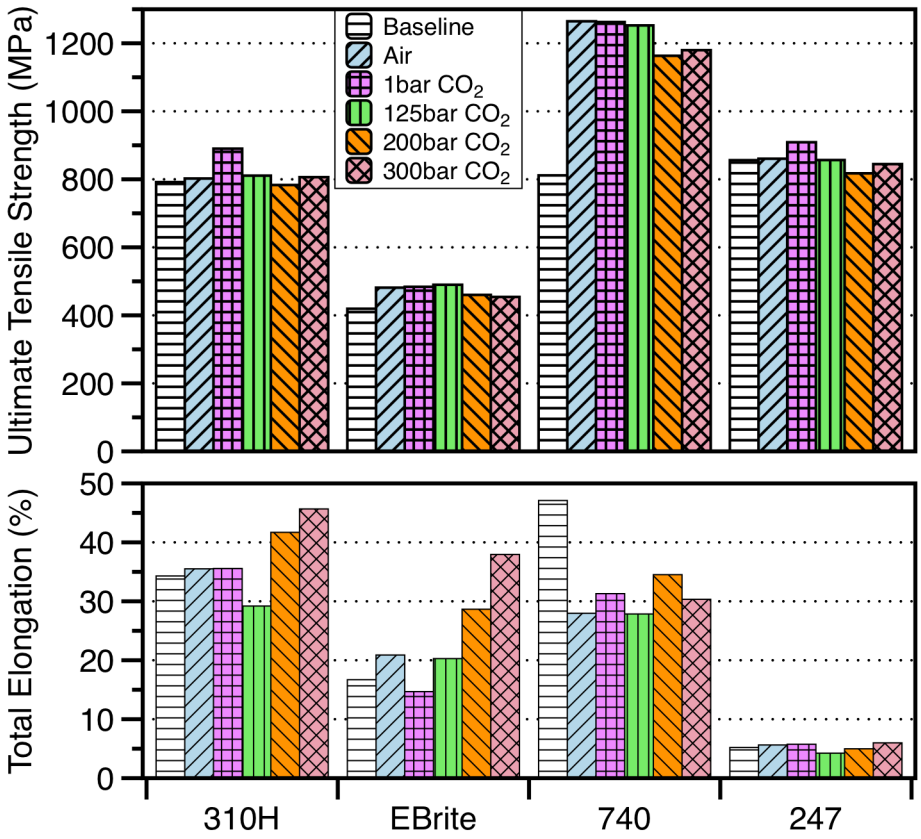

Figure 12. Room temperature tensile properties of four alloys exposed at 750°C in various environments for 500 h with a 10^{-3} s^{-1} strain rate.

DISCUSSION

All of these results should be prefaced by the limitation that these are only 500 h exposures and longer exposures, including thermal cycling, may reveal different results (e.g. accelerated reaction rates after an initial incubation period) and better differentiate, for example, the effect of pressure on compatibility. Obviously, longer exposures should enable more accurate measurements of the reaction rates and easier detection of internal carburization or other degradation mechanisms. A problem with only one exposure time is that it is not possible to differentiate transient and steady-state behavior. Thus, higher mass gains noted in Figure 8 may be due to a higher steady-state oxidation rate. However, an alloy with a higher mass gain after 500 h also could have a rapid initial or transient oxidation period followed by a steady-state oxidation rate lower than another alloy with a lower mass gain after 500h. Thus, rate constants have not been generated from these results. Likewise, internal oxidation or other morphological observations after 500h may not continue to grow at the same rate with longer exposures.

The goal of this initial work was to (1) evaluate the performance of the new autoclave and (2) use these preliminary results to assess the behavior of candidate structural alloys and design the next series of longer-term experiments. Based on these results, an initial hypothesis that pressure plays a limited role is now being evaluated by conducting long-term experiments at 0.1 and 30 MPa sCO_2. If behavior is similar in these conditions, the large compatibility database generated for CO_2-cooled nuclear reactors (1-20 kh exposures) [Evans 1976, Garrett 1982] can be utilized as well as the extensive work at ambient pressure for a variety of applications including solid oxide fuel cells and oxy-fired coal combustion. These low pressure data sets are particularly useful for

evaluating the compatibility for the direct-fired systems where high levels of O_2 and H_2O are expected and laboratory testing has not yet been developed to control impurities at >100 bar.

The exposure conditions selected for this study were partially based on prior work in the literature, Figure 1. The 125 bar condition repeated prior work at MIT [Dunlevy 2009]. The decreasing pressure at higher exposure temperatures in this study reflected the limitation of their alloy 625 autoclave. By repeating these conditions, it was possible to confirm that relatively thin reaction products were formed on the highly alloyed candidates (e.g. alloy 740) in both experiments. The current results with thick reaction products for low-alloyed stainless steels also are consistent with prior observations [e.g. Rouillard 2011]. Somewhat surprisingly, protective oxides were observed on the austenitic stainless steel 347HFG specimens with relatively low Cr and Ni contents, Table 1. This may reflect the relatively short exposure. At longer times, breakaway oxidation may occur with the formation of thick Fe-rich oxides as has been observed in other studies [Dunlevy 2009, Gheno 2012].

For the 750°C mass change results, higher mass gains were consistently shown for the alloy 282 specimens. The cross-sections in Figure 9 suggest that increased internal oxidation may explain this behavior. This alloy contains only 19%Cr and has higher Al and Ti contents for strengthening than the other chromia-forming Ni-base alloys, Table 1. How much the lower Cr content and Al and Ti internal oxidation affects the long-term behavior of this alloy in sCO_2 needs to be investigated. This alloy was exposed in long-term testing (5-10 kh) in steam and laboratory air at 800°-900°C and the depth of internal oxidation increased with relatively low parabolic kinetics [Pint 2015b].

The limited impact on mechanical properties was not surprising for the higher-alloyed materials evaluated: 310HCbN, E-Brite, 740 and 247. Additional tensile testing also may be conducted at higher temperatures and post-exposure, ex-situ evaluation of creep properties also may be conducted [Dryepondt 2012]. Recent work examined the combined effect of stress and the sCO_2 environment [Olivares 2015]. To further study this issue, future work will compare creep rupture lifetimes of Sanicro 25, 625, 740 and 282 tubes pressurized with argon and CO_2 to determine if there is a debit associated with the sCO_2 environment.

In general, somewhat limited characterization has been conducted to date on these specimens. Based on the low mass gains, relatively thin reaction products and limited Cr depletion (Figure 11) would be expected. One of the key issues to be further explored is the possible ingress of C through the external scale and whether CO_2 pressure affects this transport. The explanation for the internal attack in CO_2 is that C penetrates the scale and the C activity increases at the low O activity at the metal-scale interface where Cr/Cr_2O_3 or Al/Al_2O_3 equilibrium exists [Young 2011].

Alumina scales are thought to be less permeable to C than chromia scales [Jönsson, 1997]. However, alumina forms more readily at higher temperatures and thicker mixed scales were observed at 650°C on alloy 214 (Figure 7) and other alumina-formers [Pint 2014a]. This is a concern for sCO_2 recuperator applications where an alloy component typically will be exposed to a temperature gradient and needs to perform well at both high and low temperatures. Particularly at these relatively low exposure temperatures, the alloy Cr content helps with the selective formation of a protective Al-rich oxide [Stott 1995]. Alloy 247 has the lowest Cr content (8.5%) among the alumina-forming MCrAl-type alloys studied. A possible implication of the low Cr content is a higher mass gain associated with the initial transient formation of more base-metal containing oxides. As mentioned previously, the oxidation of the Hf-rich carbides could also contribute to the higher mass gain observed for the 247 specimens at 750°C, Figure 8.

Obviously, much more work is needed to fully understand sCO_2 material compatibility for higher temperature/pressure conditions and longer lifetime applications needed for high efficiency power generation systems. The current results are quite promising in that the reaction rates appear relatively low and no catastrophic problems have been observed for the leading structural alloy candidates at 700°-750°C. For the highest pressure and temperature conditions (>700°C/30 MPa), precipitation strengthened Ni-base superalloys like 740 [Zhao 2003, Shingledecker 2013] and 282

[Pike 2008] are the most likely candidate structural alloys with the former alloy recently gaining ASME boiler and pressure vessel code qualification and a similar code case in progress for alloy 282.

CONCLUSIONS

Initial supercritical CO_2 results have been generated with isothermal 500 h exposures at 400°-750°C (750°-1380°F) in 12-30 MPa (1800-4350 psi) CO_2. A wide range of Fe- and Ni-base alloys, which form protective Cr- and Al-rich surface oxides, has been evaluated. Many of the higher alloyed materials exhibited low mass changes and thin reaction products at all conditions. Thick Fe-rich oxides formed on 2-12%Cr steels above 400°C, consistent with previous studies. However, no indication of internal carburization was found for Grade 91 specimens exposed at 650°-750°C. Little effect of pressure on the mass change or reaction products was observed at 750°C suggesting that data generated at lower pressures may be relevant for developing lifetime model for long-term sCO_2 power generation applications. Obviously, longer-term exposures are needed to clearly identify reaction rates and verify the compatibility for these various candidate alloys in sCO_2.

NOMENCLATURE

APMT = Advanced Powder Metallurgy Tube (Sandvik/Kanthal FeCrAl alloy)
Gr. = Grade (steel)
HFG = H (high carbon) FG (fine grain structure)
ORNL = Oak Ridge National Laboratory

REFERENCES

Allam, R. J., Palmer, M. R., Brown Jr., G. W., Fetvedt, J., Freed, D., Nomoto, H., Itoh, M., Okita, N., Jones Jr., C., 2013, “High efficiency and low cost of electricity generation from fossil fuels while eliminating atmospheric emissions, including carbon dioxide,” Energy Procedia 37, 1135–1149.

Brady, M. P., Pint, B. A., Lu, Z. G., Zhu, J. H., Milliken, C. E., Kreidler, E. D.. Miller, L., Armstrong, T. R., Walker, L. R., 2006, “Comparison of Oxidation Behavior and Electrical Properties of Doped NiO- and Cr_2O_3-Forming Alloys for Solid Oxide Fuel Cell Metallic Interconnects,” Oxid. Met. 65, 237-261.

Cao, G., Firouzdor, V., Sridharan, K., Anderson, M., Allen, T. R., 2012, “Corrosion of austenitic alloys in high temperature supercritical carbon dioxide,” Corros. Sci. 60, 246-255.

Chen, H., Goswami, D. Y., Stefanakos, E. K., 2010, “A review of thermodynamic cycles and working fluids for the conversion of low-grade heat,” Renewable & Sustainable Energy Reviews 14, 3059-3067.

Dostal, V., Hejzlar, P., Driscoll, M. J., 2006, “The supercritical carbon dioxide power cycle: Comparison to other advanced power cycles,” Nuclear Technology, 154(3), 283-301.

Dryepondt, S., Unocic K. A., Pint, B. A., 2012, “Effect of Steam Exposure on the Creep Properties of Ni-based Alloys,” Mater. Corros. 63, 889-895.

Dunlevy, M. W., 2009, “An Exploration of the Effect of Temperature on Different Alloys in Supercritical Carbon Dioxide Environment,” M.Sc. Thesis, MIT, Cambridge, MA.

Ennis P. J., Quadakkers, W. J., 1985, “Corrosion and Creep of Nickel-Base Alloys in Steam Reforming Gas,” in High Temperature Alloys, Their Exploitable Potential, eds. J. B. Marriott, M. Merz, J. Nihoul and J. Ward, Elsevier, London, p.465-74.

Evans, H. E., Hilton, D. A., Holm, R. A., 1976, “Chromium-Depleted Zones and the Oxidation Process in Stainless Steels,” Oxid. Met. 10, 149-161.

Firouzdor, V. Sridharan, K., Cao, G., Anderson, M. Allen, T. R., 2013, “Corrosion of a stainless

steel and nickel-based alloys in high temperature supercritical carbon dioxide environment," Corros. Sci. 69, 281-291.

Garrett, J. C. P., Crook, J. T., Lister, S. K., Nolan, P. J., Twelves, J. A., 1982, "Factors in the Oxidation Assessment of AISI Type 310 Steels in High Pressure Carbon Dioxide," Corros. Sci. 22, 37-50.

Gheno, T., Monceau, D., Young, D. J., 2012, "Mechanism of breakaway oxidation of Fe-Cr and Fe-Cr-Ni alloys in dry and wet carbon dioxide," Corros. Sci., 64, 222-233.

Gibbs, J. P., 2010, "Corrosion of Various Engineering Alloys in Supercritical Carbon Dioxide Environment," M.Sc. Thesis, MIT, Cambridge, MA.

He, L. F., Roman, P., Leng, B., Sridharan, K., Anderson, M. Allen, T. R., 2014, "Corrosion behavior of an alumina forming austenitic steel exposed to supercritical carbon dioxide," Corros. Sci. 82, 67–76.

Iverson, B. D., Conboy, T. M., Pasch, J. J., Kruizenga, A. M., 2013, "Supercritical CO_2 Brayton cycles for solar-thermal energy," Applied Energy, 111, 957-970.

Jönsson, B., Svedberg, C., 1997, "Limiting Factors for Fe-Cr-Al and NiCr in Controlled Industrial Atmospheres," Mater. Sci. Forum, 251-254 (1997) 551-558.

McCoy, H. E., 1965, "Type 304 Stainless Steel vs Flowing CO_2 at Atmospheric Pressure and 1100-1800°F," Corros., 21, 84-94.

Moore, R., Conboy, T., 2012, "Metal Corrosion in a Supercritical Carbon Dioxide – Liquid Sodium Power Cycle," Sandia National Laboratory Report SAND2012-0184.

Oh, C. H., Lillo, T., Windes, W., Totemeier, T., Ward, B., Moore, R., Barner, R., 2006, "Development Of A Supercritical Carbon Dioxide Brayton Cycle: Improving VHTR Efficiency And Testing Material Compatibility," Idaho National Laboratory Report INL/EXT-06-01271.

Olivares, R. I., Young, D. J., Marvig, P., Stein, W., 2015, "Alloys SS316 and Hastelloy-C276 in Supercritical CO_2 at High Temperature," Oxid. Met. 84, 585–606.

Pike, L. M., 2008, "Development of a Fabricable Gamma-Prime (γ') Strengthened Superalloy," in *Superalloys 2008*, R. C. Reed et al. eds TMS, Warrendale, PA, 2008, p.191-200.

Pint B. A., Keiser, J. R., 2014a, "The Effect of Temperature on the sCO_2 Compatibility of Conventional Structural Alloys," in Proceedings of the 4th International Symposium on Supercritical CO_2 Power Cycles, Pittsburgh, PA, September 2014, Paper #61.

Pint, B. A., 2014b, "The Use of Model Alloys to Study the Effect of Alloy Composition on Steam and Fireside Corrosion," NACE Paper 14-4279, Houston, TX, presented at NACE Corrosion 2014, San Antonio, TX.

Pint, B. A., Thomson, J. K., 2014c, "Effect of oxy-firing on corrosion rates at 600°-650°C," Mater. Corros. 65, 132-140.

Pint B. A., Keiser, J. R., 2015a, "Initial Assessment of Ni-Base Alloy Performance in 0.1 MPa and Supercritical CO_2," JOM 67(11), 2615-2620.

Pint, B. A., Thiesing, B. P., 2015b, "Effect of Environment on the Oxidation Behavior of Commercial and Model Ni-Base Alloys," NACE Paper C2015-5919, Houston, TX, presented at NACE Corrosion 2015, Dallas, TX.

Pint B. A., Brese, R. G., Keiser, J. R., 2016a, "Supercritical CO_2 Compatibility of Structural Alloys at 400°-750°C," NACE Paper C2016-7747, Houston, TX, presented at NACE Corrosion 2016, Vancouver, Canada, March 2016.

Pint B. A., Brese, R. G., Keiser, J. R., 2016b, "Effect of Pressure on Supercritical CO_2 Compatibility of Structural Alloys at 750°C," Mater. Corros. in press.

Quadakkers, W. J., Olszewski, T., Piron-Abellan, J., Shemet, V., Singheiser, L., 2011, “Oxidation of Metallic Materials in Simulated CO_2/H_2O-rich Service Environments Relevant to an Oxyfuel Plant,” Mater. Sci. Forum 696, 194-199.

Rouillard, F., Charton, F., Moine, G., 2011 “Corrosion Behavior of Different Metallic Materials in Supercritical Carbon Dioxide at 550°C and 250 bars,” Corros. 67(9), 095001

Shingledecker, J. P., Pharr, G. M., 2013, “Testing and Analysis of Full-Scale Creep-Rupture Experiments on Inconel Alloy 740 Cold-Formed Tubing,” J. Mater. Eng. Perform., 22, 454-462.

Stott, F. H., Wood, G. C., Stringer, J., 1995, "The Influence of Alloying Elements on the Development and Maintenance of Protective Scales," Oxid. Met. 44, 113-145.

Tan, L., Anderson, M., Taylor, D., Allen, T. R., 2011, “Corrosion of austenitic and ferritic-martensitic steels exposed to supercritical carbon dioxide,” Corros. Sci. 53, 3273-3280.

Viswanathan, R., Henry, J.F., Tanzosh, J., Stanko, G., Shingledecker, J., Vitalis, B., Purgert, R., 2005, “U.S. Program on Materials Technology for Ultra-Supercritical Coal Power Plants,” J. Mater. Eng. Performance 14(3), 281-285.

Viswanathan, R., Shingledecker, J., Purgert, R., 2010, “Evaluating Materials Technology for Advanced Ultrasupercritical Coal-Fired Plants,” Power, 154(8), 41-45.

Wright, I. G., Dooley, R. B., 2010, “A review of the oxidation behavior of structural alloys in steam,” International Mater. Rev. 55 (3), 129-167.

Wright, I. G., Pint, B. A., Shingledecker, J. P., Thimsen, D., 2013, “Materials Considerations for Supercritical CO_2 Turbine Cycles,” ASME Paper #GT2013-94941, presented at the International Gas Turbine & Aeroengine Congress & Exhibition, San Antonio, TX, June, 3-7, 2013.

Young, D. J., Zhang, J., Geers C., Schütze, M., 2011, “Recent advances in understanding metal dusting: A review,” Mater. Corros. 62, 7-28.

Zhang, X. R., Yamaguchi, H., Uneno, D., Fujima, K., Enomoto, M., Sawada, N. , 2006, “Analysis of a novel solar energy-powered Rankine cycle for combined power and heat generation using supercritical carbon dioxide,” Renewable Energy, 31, 1839-1854.

Zhao, S. Q., Xie, X. S., Smith, G. D. Patel, S. J., 2003, “Microstructural stability and mechanical properties of a new nickel based superalloy,” Mater. Sci. Eng. A 355, 96-105.

ACKNOWLEDGEMENTS

The experimental work at ORNL was conducted by M. Howell, M. Stephens, T. Lowe and T. Jordan. Material was provided by Haynes International, Special Metals, Allegheny-Ludlum, Sumitomo Metals, Capstone Turbines, Sandvik (Kanthal). M. G. Frith provided useful comments on the manuscript. Research sponsored by the U. S. Department of Energy, Office of Fossil Energy, Coal and Power R&D. This manuscript has been authored by UT-Battelle, LLC under Contract No. DE-AC05-00OR22725 with the U.S. Department of Energy. The United States Government retains and the publisher, by accepting the article for publication, acknowledges that the United States Government retains a non-exclusive, paid-up, irrevocable, world-wide license to publish or reproduce the published form of this manuscript, or allow others to do so, for United States Government purposes. The Department of Energy will provide public access to these results of federally sponsored research in accordance with the DOE Public Access Plan (http://energy.gov/downloads/doe-public-access-plan).